Editors' Suggestion | Featured in Physics

Experimental Test of the Differential Fluctuation Theorem and a Generalized Jarzynski Equality for Arbitrary Initial States

Thai M. Hoang,[1,*] Rui Pan,[2] Jonghoon Ahn,[3] Jaehoon Bang,[3] H. T. Quan,[2,4,†] and Tongcang Li[1,3,5,6,‡]
[1]*Department of Physics and Astronomy, Purdue University, West Lafayette, Indiana 47907, USA*
[2]*School of Physics, Peking University, Beijing 100871, People's Republic of China*
[3]*School of Electrical and Computer Engineering, Purdue University, West Lafayette, Indiana 47907, USA*
[4]*Collaborative Innovation Center of Quantum Matter, Beijing 100871, People's Republic of China*
[5]*Purdue Quantum Center, Purdue University, West Lafayette, Indiana 47907, USA*
[6]*Birck Nanotechnology Center, Purdue University, West Lafayette, Indiana 47907, USA*

(Received 7 October 2017; published 22 February 2018)

Nonequilibrium processes of small systems such as molecular machines are ubiquitous in biology, chemistry, and physics but are often challenging to comprehend. In the past two decades, several exact thermodynamic relations of nonequilibrium processes, collectively known as fluctuation theorems, have been discovered and provided critical insights. These fluctuation theorems are generalizations of the second law and can be unified by a differential fluctuation theorem. Here we perform the first experimental test of the differential fluctuation theorem using an optically levitated nanosphere in both underdamped and overdamped regimes and in both spatial and velocity spaces. We also test several theorems that can be obtained from it directly, including a generalized Jarzynski equality that is valid for arbitrary initial states, and the Hummer-Szabo relation. Our study experimentally verifies these fundamental theorems and initiates the experimental study of stochastic energetics with the instantaneous velocity measurement.

DOI: 10.1103/PhysRevLett.120.080602

In the past two decades, there were significant developments in nonequilibrium statistical mechanics of small systems in which thermal fluctuation is influential [1]. The most prominent progress is the discovery of various fluctuation theorems (FTs), which connect microscopic dynamics with thermodynamic behaviors [1]. These FTs, such as the Jarzynski equality (JE) [2,3] and the Crooks fluctuation theorem (CFT) [4,5], reformulate the inequality of the second law into equalities and reveal the universal laws that the fluctuating thermodynamic variables must obey in processes arbitrarily far from thermal equilibrium. As they are refinements of the second law on individual trajectories, they provide critical understanding of behaviors of biological systems at the single molecular level [3,5–10] and nonequilibrium dynamics of a wide range of physical systems [11–28]. While JE and CFT are valid for processes far from thermal equilibrium, they require the initial state to be in a thermal equilibrium state.

In 2000, a differential fluctuation theorem (DFT) connecting the joint probabilities of entropy production and arbitrary generalized coordinates (e.g., position and velocity coordinates) was derived by Jarzynski [29]. An equivalent DFT for work was derived by Nobel laureate Karplus and co-workers in 2008 [20]. It is remarkable that the DFT can unify various FTs as long as detailed balance is not violated [20] (see Fig. S1 in the Supplemental Material [30] for the relation between different fluctuation theorems). The DFT also leads to a generalized Jarzynski equality (GJE) for arbitrary initial states [24]. Such an ability is rooted from the fact that most FTs originate from the same fundamental principle: the microscopic reversibility connecting forward and reverse trajectories [1,18,24,29,31–33]. Testing the DFT and other FTs would deepen our understanding of the second law and nonequilibrium physics, including dissipation [19], hysterisis [34], and irreversibility [35]. In order to test the DFT at its desired level of detail, we need large statistics and the ability to track individual trajectories of a stochastic process in the phase space [20], which requires the measurement of instantaneous velocities of Brownian motion [36].

In this work, we experimentally test the differential fluctuation theorem [20,29] using an optically levitated nanosphere which can be trapped in air continuously for weeks for acquiring large sets of data. Our ultrasensitive optical tweezer can measure both instantaneous position and instantaneous velocity [36] of a levitated nanosphere to test DFT. Over one million experimental cycles per setting ($\sim 10^{10}$ position data points per setting with a 10-MHz acquisition rate) provide sufficient statistics to validate the DFT at its desired level of detail, e.g., testing DFT for nonequilibrium processes connecting two points in the position-velocity space [20]. Several fluctuation theorems, including the JE [2,3], the CFT [4,5], the Hummer-Szabo relation (HSR) [6–8], the GJE [19,24,31], the extended fluctuation relation (EFR) [9,10], and the fluctuation theorem for ligand binding (FTLB) [37] can be unified

by the DFT [18,24,31,32]. We have also tested several such theorems. In our experiment, the air pressure can be adjusted to test these theorems in both underdamped and overdamped regimes. This study demonstrates a powerful approach applicable in exploring a wide range of nonequilibrium systems [3,5–13,15,16] since a complete description of the stochastic system includes the information of both position and velocity.

Our experiments are carried out using a silica nanosphere levitated by a 1550-nm optical tweezer [Fig. 1(a)] [38]. The nonequilibrium processes are controlled by a force parameter f which is an optical force exerted on the nanosphere by a 532-nm laser beam. In a forward process, the optical force is ramped from $f_{\rm off}$ at time t_1 to $f_{\rm on}$ at time t_2. The reverse process is from t_3 to t_4. The DFT connects the forward and reverse processes as [20,29]

$$P_R(-W, b^* \to a^*)/P_F(W, a \to b) = e^{-\beta(W-\Delta F)}, \quad (1)$$

where a, b can be arbitrary generalized coordinates. In our work, a and b denote the position (x) and/or velocity (v) coordinate of a levitated nanosphere; e.g., a can be x, or v, or (x, v). $P_F(W, a \to b)$ is the forward joint probability of performing nonequilibrium work W for those trajectories starting from a and ending at b, and $P_R(-W, b^* \to a^*)$ is the reverse joint probability. The work distribution $P_F(W)$ can be obtained by integrating $P_F(W, a \to b)$ over a and b. The asterisk (*) denotes a reversal of the velocity components of a or b. $\Delta F = -(f_{\rm on}^2 - f_{\rm off}^2)/(2k)$ is the free energy difference between the equilibrium states of the optical forces $f_{\rm on}$ and $f_{\rm off}$. Here, k is the trap stiffness $\beta = 1/(k_B T)$, where k_B is the Boltzmann constant, and $T = 296$ K is the room temperature.

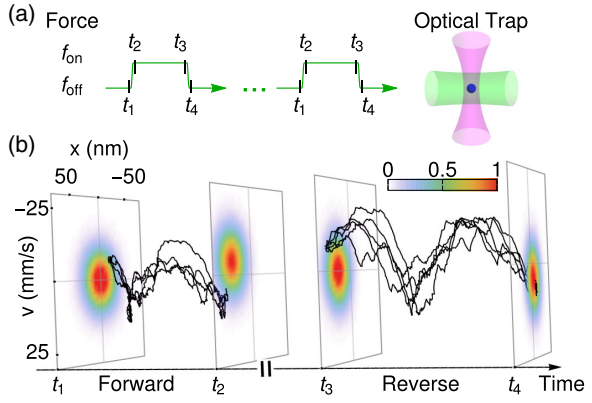

FIG. 1. (a) Experimental scheme. A silica nanosphere (blue sphere) is trapped in an optical tweezer formed by a focused 1550-nm laser beam (magenta). A series of 532-nm laser pulses (green) exerts an optical force on the nanosphere to drive nonequilibrium processes. Within each pulse, an optical force is rapidly ramped from $f_{\rm off}$ at time t_1 to $f_{\rm on}$ at time t_2 during the forward process (green pulse). The reverse process from time t_3 to t_4 is the time-reversed correspondence of the forward process. (b) An example of experimental data. Vertical slides represent the measured time snapshots of the probability distributions at times t_1, t_2, t_3, and t_4 as illustrated in (a). Black curves represent experimental phase-space trajectories during forward processes initialized at (x_1, v_1) and finalized at (x_2, v_2), and during reverse processes initialized at the $(x_2, -v_2)$ and finalized at $(x_1, -v_1)$. Here, $x_1 = -19$ nm, $x_2 = 55$ nm, $v_1 = -7$ mm/s, and $v_2 = 7$ mm/s. The nanosphere is levitated in air at 50 torr, and $f_{\rm off} = 0$, $f_{\rm on} = 340$ fN.

To test the DFT in detail, over one million experimental forward-reverse cycles (500 μs/cycle) are performed for a given irreversible setting. Their distributions in the position-velocity space are shown in Fig. 1(b). The driving optical forces significantly shift the distributions away from the undriven ones. The black curves in Fig. 1(b) are a few examples of measured trajectories evolving from a given point to a different point in the phase space during forward (or reverse) processes. Because of thermal fluctuation, it is not possible to have two trajectories starting from exactly the same point in the phase space. Here we use (x, v) to represent points within $(x \pm (\sigma_x/11), v \pm (\sigma_v/11))$, where σ_x and σ_v are the standard deviations of the position and velocity distributions, respectively.

Based on our large sets of experimental data and our ability to measure both the instantaneous velocity and position of a nanoparticle, we develop an efficient method to prepare arbitrary nonequilibrium initial states by conditionally selecting trajectories that start from the desired initial states. Some examples of arbitrary nonequilibrium initial states prepared by our information-based method are shown in Fig. 2. They are used to test the DFT and the GJE for arbitrary initial states.

Figure 3 shows our experimental results of testing DFT with a 209-nm-radius nanopshere in the underdamped regime (see the Supplemental Material [30] for more information). The optical force [Fig. 3(a)] is monitored using a fraction of the 532-nm laser split from the main beam. Figures 3(b) and 3(c) show the dynamic evolution of the nanosphere in the position and velocity coordinates, respectively. Since the irreversible ramps (~4.6 μs) are faster than the velocity (~8.6 μs) and position (~100 μs) relaxation times, the nanosphere is far from thermal equilibrium when the ramps finish.

With the acquired position, velocity, and force data, the DFT is ready to be tested. The DFT in Eq. (1) can be rewritten in the position coordinate as $[(P_R(-W, x_2 \to x_1))/(P_F(W, x_1 \to x_2))] = [(P_R(x_2 \to x_1))/(P_F(x_1 \to x_2))] \times [(P_R(-W|x_2 \to x_1))/(P_F(W|x_1 \to x_2))]$ [20]. Here, $P_F(x_1 \to x_2)$ is the probability of having a forward trajectory going from x_1 to x_2, and $P_R(x_2 \to x_1)$ is the probability of a reverse trajectory going from x_2 to x_1. These quantities can be calculated using the distributions illustrated in Fig. 1(b). They are essentially equivalent to the number of forward (reverse) trajectories going from x_1 to x_2 (x_2 to x_1). $P_F(W|x_1 \to x_2)$ is the probability of performing work W for those forward trajectories going from x_1 to x_2, and $P_R(-W|x_2 \to x_1)$ is the reverse probability [Fig. 3(d)].

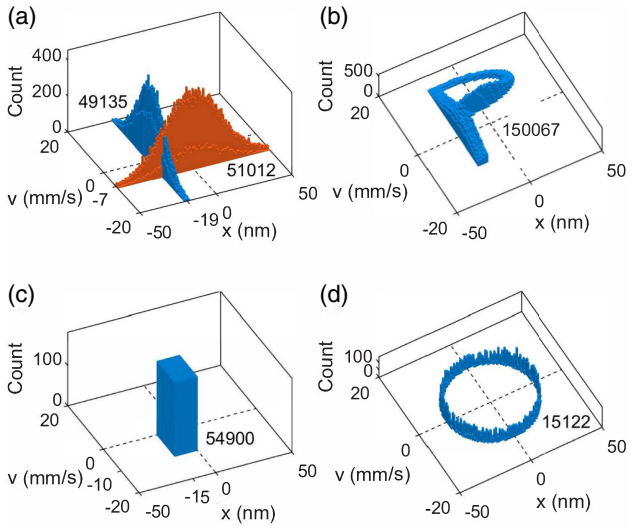

FIG. 2. Examples of arbitrary nonequilibrium initial states of trajectory ensembles prepared by an information-based method. (a) Nonequilibrium initial states with narrow distributions in position or velocity. (b) An exotic nonequilibirum state with a P-shaped distribution in the phase space. (c) Uniform distribution within a rectangle (-15 nm $< x < 0$, -10 mm/s $< v < 0$) in the phase space. (d) A microcanonical ensemble with the energy shell $1.3k_BT < E < 1.35k_BT$. The number of experimental trajectories started from each nonequilibrium initial state is labeled next to its distribution.

Similarly, Fig. 3(e) shows examples of $P_F(W|v_1 \to v_2)$ and $P_R(-W|-v_2 \to -v_1)$ in the velocity coordinate. The minus sign $(-)$ in the velocity space is due to the time reversal symmetry of the reverse process. Here, irreversible work is calculated as $W = -\sum_{i=1}^{n-1}(f_{i+1} - f_i)(x_i + x_{i+1})/2$ for n successive position and force measurements. This formula is obtained using the Hamiltonian $H = \frac{1}{2}kx^2 - fx + \frac{1}{2}mv^2$ and the work definition $W = \int_0^\tau dt\dot{f}(t)[(\partial H)/(\partial f)]$ during a ramp period τ [2].

The DFT is tested in detail using 121 different initial-final combinations in the position and velocity coordinates uniformly distributed in $(\pm\sigma_x, \pm\sigma_v)$. Figure 3(f) shows that the left-hand side $[(P_R(-W, x_2 \to x_1))/(P_F(W, x_1 \to x_2))]$ agrees well with the right-hand side $e^{-\beta(W-\Delta F)}$ of the DFT in Eq. (1). Here, $e^{-\beta(W-\Delta F)}$ is a function of the work variable W. The free energy difference can be calculated as $\Delta F = -1.3k_BT$ with $f_{\rm off}/f_{\rm on} = 0/340$ fN [Fig. 3(a)]. Similarly, we can verify the DFT in the velocity coordinate [Fig. 3(g)]. Data points also distribute closely to the curves $e^{-\beta(W-\Delta F)}$. Thus, our data agree with the DFT well in position and velocity coordinates simultaneously.

Our experimental data can also test other fluctuation theorems which are direct integrations of the DFT [30]. Integrating Eq. (1) over W and b, we obtain the GJE for delta initial distributions in the position or velocity coordinates ($a = x$ or $a = v$) [19,24,31],

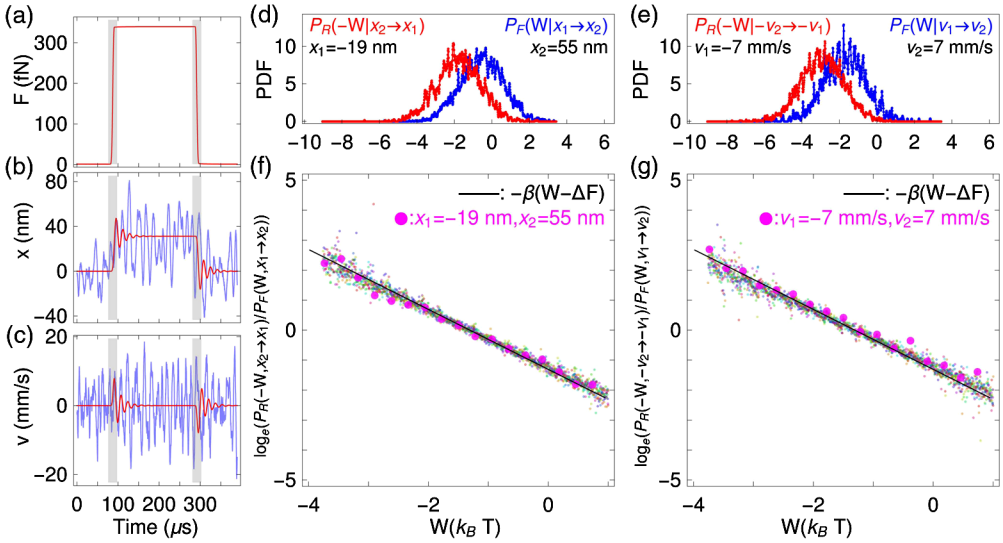

FIG. 3. Testing the differential fluctuation theorem in the underdamped regime. (a) Optical force. (b),(c) Measured position and velocity trajectories. A single trajectory is shown in blue, and the averaged trajectory of over one million trajectories is shown in red. The gray shaded regions in (a)–(c) denote the forward and reverse intervals, respectively. It takes roughly 4.6 μs for the optical force strength to switch from the 10% to 90% level. (d) An example of probabilities $P_F(W|x_1 \to x_2)$ and $P_R(-W|x_2 \to x_1)$ in position coordinate. (e) An example of probabilities $P_F(W|v_1 \to v_2)$ and $P_R(-W|-v_2 \to -v_1)$ in velocity coordinate. The label of the horizontal axis in (d) and (e) is $W(k_BT)$. (f),(g) Testing the DFT in position and velocity spaces. The small markers with different colors represent measurements of $\log_e[(P_R(-W, x_2 \to x_1))/(P_F(W, x_1 \to x_2))]$ and $\log_e[(P_R(-W, -v_2 \to -v_1))/(P_F(W, v_1 \to v_2))]$ for 121 different $\{x_1, x_2\}$ and $\{v_1, v_2\}$ combinations, respectively. The big magenta markers are results for parameters shown in (d) and (e), respectively. The black lines represent $-\beta(W - \Delta F)$.

$$\langle e^{-\beta(W-\Delta F)}|x_i = x\rangle_F = P_R(x_f = x)/P_F(x_i = x),$$
$$\langle e^{-\beta(W-\Delta F)}|v_i = v\rangle_F = P_R(v_f = -v)/P_F(v_i = v). \quad (2)$$

Here, $P_F(x_i = x)$ is the probability that a forward trajectory *initializes* at x, and $P_R(x_f = x)$ is the probability that a reverse trajectory *finalizes* at x. We use subscripts "i" and "f" to denote "initial" and "final," respectively. Similarly, $P_F(v_i = v)$ and $P_R(v_f = -v)$ are the probabilities in the velocity coordinate. They are proportional to the number of trajectories *initialized* (*finalized*) at x or v [Fig. 2(a)]. The value $\langle e^{-\beta(W-\Delta F)}|x_i = x(\text{or } v_i = v)\rangle_F$ is averaged over all forward trajectories initialized at x or v in the position or velocity coordinates. The data agree well with the GJE as shown in Figs. 4(a) and 4(b). For slow ramps, the measured $\langle e^{-\beta(W-\Delta F)}|x_i(\text{or } v_i)\rangle_F$ stays closely to 1, which is the result of a reversible process. However, for fast (irreversible) ramps, the values of $\langle e^{-\beta(W-\Delta F)}|x_i(\text{or } v_i)\rangle_F$ diverge away from 1, so the GJE is needed to explain our observations.

Similarly, integrating Eq. (1) over W and a leads to the HSR [30] in the position and velocity spaces ($b = x$ or $b = v$) [6,19,20],

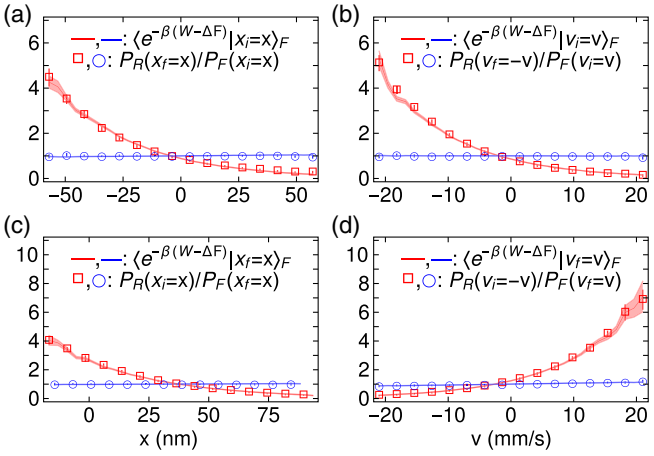

FIG. 4. Testing fluctuation theorems in the underdamped regime. (a),(b) Testing GJE in position and velocity spaces for a fast ramp (red, 4.6 μs from 10% to 90% levels) and a slow ramp (blue, 40 μs from 10% to 90% levels). Markers represent the measured $P_R(x_f = x)/P_F(x_i = x)$ and $P_R(v_f = -v)/P_F(v_i = v)$ in position and velocity spaces, respectively. (c),(d) Testing HSR in position and velocity spaces for a fast ramp (red) and a slow ramp (blue). Markers represent the measured $P_R(x_i = x)/P_F(x_f = x)$ and $P_R(v_i = -v)/P_F(v_f = v)$ in position and velocity spaces, respectively. The error bars of $P_R(x)/P_F(x)$ and $P_R(-v)/P_F(v)$ represent the standard deviation of the measurements for 20 equal divisions in each subset x and v, respectively. The markers represent their mean values. In (a)–(d), the shaded line represents $\langle e^{-\beta(W-\Delta F)}\rangle$, where its thickness represents the uncertainty of 600 work (Joule) calibrations.

$$\langle e^{-\beta(W-\Delta F)}|x_f = x\rangle_F = P_R(x_i = x)/P_F(x_f = x),$$
$$\langle e^{-\beta(W-\Delta F)}|v_f = v\rangle_F = P_R(v_i = -v)/P_F(v_f = v). \quad (3)$$

Here, $\langle e^{-\beta(W-\Delta F)}|x_f = x(\text{or } v_f = v)\rangle_F$, $P_F(x_f = x)$, and $P_R(x_i = x)$ are denoted using the same conventions as in the GJE in Eq. (2). The data agree well with the HSR for both fast (irreversible) ramps and slow (reversible) ramps as shown in Figs. 4(c) and 4(d).

Integrating Eq. (2) over initial phase-space points with an arbitrary initial distribution, one obtains the GJE for arbitrary initial states proposed in Ref. [24]

$$\langle e^{-\beta(W-\Delta F)}\rangle_{P_{\text{ini}}(x_i,v_i)} = \int \frac{P_R(x_f = x, v_f = -v)}{P_F(x_i = x, v_i = v)} \times P_{\text{ini}}(x_i = x, v_i = v)dxdv, \quad (4)$$

where $P_{\text{ini}}(x_i, v_i)$ indicates an arbitrary initial distribution in phase space. We test Eq. (4) for the thermal equilibrium initial state and three representative nonequilibrium initial states as shown in Figs. 2(b)–2(d). The results are shown in Table I. The left-hand side (lhs) and right-hand side (rhs) of Eq. (4) agree well with each other within the experimental uncertainty.

With our experimental data, we can test JE [2] and CFT [4] with high precision. The results are shown in Fig. S2 in the Supplemental Material [30]. For completeness, we also tested the DFT in the overdamped regime ($a = x_1$ and $b = x_2$) where the velocity relaxes to equilibrium much faster than other processes. As shown in Fig. S3 in the Supplemental Material [30], our experimental data show good agreement with HSR [6], the DFT [20], and the GJE [19,24]. Overall, the differential fluctuation theorem unifies many existing fluctuation theorems [9,10,18,24,31,32,37], such as JE, CFT, HSR, GJE, EFR, and FTLB, and is arguably the most detailed fluctuation theorem that can be tested experimentally. The DFT can also improve free energy calculations [20]. Our experimental results validate the DFT [20] well in both underdamped and overdamped regimes. Our work deepens our understanding of the second law to an unprecedentedly detailed level. It initiates the experimental study of stochastic thermodynamics with

TABLE I. Test of the GJE for arbitrary initial states. The thermal equilibrium state and three representative nonequilibrium initial states shown in Figs. 2(b)–2(d) are chosen for the test. The second and third rows show the data of the lhs and rhs of Eq. (4) for each initial state, respectively.

Initial state	Thermal equilibrium	P-shaped state [Fig. 2(b)]	Uniform distribution [Fig. 2(c)]	Microcanonical ensemble [Fig. 2(d)]
lhs	1.02 ± 0.02	0.92 ± 0.02	1.42 ± 0.03	1.08 ± 0.02
rhs	1	0.90	1.42	1.07

instantaneous velocity measurements and may shed new light on our understanding of the origin of time's arrow [34]. Once cooled to the quantum regime, a levitated nanosphere in vacuum can be used to investigate quantum nonequilibrium thermodynamics in the mesoscopic regime [39]. This system can also be used to study the effects of geometry in thermodynamic control [40].

T. L. acknowledges support from National Science Foundation under Grant No. PHY-1555035 and the Tellabs Foundation. H. T. Q. acknowledges support from the National Science Foundation of China under Grants No. 11375012 and No. 11534002, and The Recruitment Program of Global Youth Experts of China.

*Present address: Sandia National Laboratories, Albuquerque, NM 87123, USA.
†Corresponding author.
htquan@pku.edu.cn
‡Corresponding author.
tcli@purdue.edu

[1] C. Jarzynski, Annu. Rev. Condens. Matter Phys. **2**, 329 (2011).
[2] C. Jarzynski, Phys. Rev. Lett. **78**, 2690 (1997).
[3] J. Liphardt, S. Dumont, S. B. Smith, I. Tinoco, and C. Bustamante, Science **296**, 1832 (2002).
[4] G. E. Crooks, Phys. Rev. E **60**, 2721 (1999).
[5] D. Collin, F. Ritort, C. Jarzynski, S. B. Smith, I. Tinoco, and C. Bustamante, Nature (London) **437**, 231 (2005).
[6] G. Hummer and A. Szabo, Proc. Natl. Acad. Sci. U.S.A. **98**, 3658 (2001).
[7] N. C. Harris, Y. Song, and C.-H. Kiang, Phys. Rev. Lett. **99**, 068101 (2007).
[8] A. N. Gupta, A. Vincent, K. Neupane, H. Yu, F. Wang, and M. T. Woodside, Nat. Phys. **7**, 631 (2011).
[9] I. Junier, A. Mossa, M. Manosas, and F. Ritort, Phys. Rev. Lett. **102**, 070602 (2009).
[10] A. Alemany, A. Mossa, I. Junier, and F. Ritort, Nat. Phys. **8**, 688 (2012).
[11] G. M. Wang, E. M. Sevick, E. Mittag, D. J. Searles, and D. J. Evans, Phys. Rev. Lett. **89**, 050601 (2002).
[12] E. Trepagnier, C. Jarzynski, F. Ritort, G. E. Crooks, C. Bustamante, and J. Liphardt, Proc. Natl. Acad. Sci. U.S.A. **101**, 15038 (2004).
[13] F. Douarche, S. Joubaud, N. B. Garnier, A. Petrosyan, and S. Ciliberto, Phys. Rev. Lett. **97**, 140603 (2006).
[14] Y. Jun, M. Gavrilov, and J. Bechhoefer, Phys. Rev. Lett. **113**, 190601 (2014).
[15] J. Gieseler, R. Quidant, C. Dellago, and L. Novotny, Nat. Nanotechnol. **9**, 358 (2014).
[16] D. Y. Lee, C. Kwon, and H. K. Pak, Phys. Rev. Lett. **114**, 060603 (2015).
[17] J. P. Pekola, Nat. Phys. **11**, 118 (2015).
[18] U. Seifert, Phys. Rev. Lett. **95**, 040602 (2005).
[19] R. Kawai, J. M. R. Parrondo, and C. Van den Broeck, Phys. Rev. Lett. **98**, 080602 (2007).
[20] P. Maragakis, M. Spichty, and M. Karplus, J. Phys. Chem. B **112**, 6168 (2008).
[21] M. Esposito and C. Van den Broeck, Phys. Rev. Lett. **104**, 090601 (2010).
[22] T. Sagawa and M. Ueda, Phys. Rev. Lett. **104**, 090602 (2010).
[23] S. Toyabe, T. Sagawa, M. Ueda, E. Muneyuki, and M. Sano, Nat. Phys. **6**, 988 (2010).
[24] Z. Gong and H. T. Quan, Phys. Rev. E **92**, 012131 (2015).
[25] V. Blickle, T. Speck, L. Helden, U. Seifert, and C. Bechinger, Phys. Rev. Lett. **96**, 070603 (2006).
[26] I. A. Martinez, E. Roldan, L. Dinis, D. Petrov, J. M. R. Parrondo, and R. A. Rica, Nat. Phys. **12**, 67 (2016).
[27] A. Bérut, A. Petrosyan, and S. Ciliberto, Europhys. Lett. **103**, 60002 (2013).
[28] J. V. Koski, V. F. Maisi, T. Sagawa, and J. P. Pekola, Phys. Rev. Lett. **113**, 030601 (2014).
[29] C. Jarzynski, J. Stat. Phys. **98**, 77 (2000).
[30] See the Supplemental Material at http://link.aps.org/supplemental/10.1103/PhysRevLett.120.080602 for the relation between various FTs, the test of JE and CFT, the calibration method, and results in the overdamped regime.
[31] G. E. Crooks, Ph. D. thesis, University of California, Berkeley, 1999.
[32] C. V. den Broeck, Stochastic thermodynamics: A brief introduction, in *Physics of Complex Colloids*, edited by C. Bechinger, F. Sciortino, and P. Ziherl (IOS Press, Amsterdam, 2013), pp. 155–194.
[33] U. Seifert, Rep. Prog. Phys. **75**, 126001 (2012).
[34] E. H. Feng and G. E. Crooks, Phys. Rev. Lett. **101**, 090602 (2008).
[35] A. Gomez-Marin, J. M. R. Parrondo, and C. Van den Broeck, Europhys. Lett. **82**, 50002 (2008).
[36] T. Li, S. Kheifets, D. Medellin, and M. G. Raizen, Science **328**, 1673 (2010).
[37] J. Camunas-Soler, A. Alemany, and F. Ritort, Science **355**, 412 (2017).
[38] T. M. Hoang, J. Ahn, J. Bang, and T. Li, Nat. Commun. **7**, 12250 (2016).
[39] Z.-q. Yin, A. A. Geraci, and T. Li, Int. J. Mod. Phys. B **27**, 1330018 (2013).
[40] P. R. Zulkowski, D. A. Sivak, G. E. Crooks, and M. R. DeWeese, Phys. Rev. E **86**, 041148 (2012).